A mechanism for weak itinerant antiferromagnetism: Mirrored van Hove singularities

2016 EPL 116 27004

(http://iopscience.iop.org/0295-5075/116/2/27004)

A Letters Journal Exploring the Frontiers of Physics

October 2016

EPL, **116** (2016) 27004
doi: 10.1209/0295-5075/116/27004

www.epljournal.org

A mechanism for weak itinerant antiferromagnetism: Mirrored van Hove singularities

Wen Fong Goh and Warren E. Pickett

Department of Physics, University of California - Davis, CA 95616, USA

received 28 September 2016; accepted 7 November 2016
published online 1 December 2016

PACS 75.10.-b – General theory and models of magnetic ordering
PACS 71.20.-b – Electron density of states and band structure of crystalline solids
PACS 71.20.Be – Transition metals and alloys

Abstract – Unlike the other prominent macroscopic spin-paired quantum state, superconductivity, where the focus is on the strongest coupling within a class, untuned weak magnetism presents an intellectual frontier where electronic structure, magnetic coupling, and (quantum and thermal) fluctuations provide a platform for unconventional phenomena. With a strong van Hove singularity (vHs) at the Fermi energy, TiAu (with no magnetic element) is highly unstable toward ferromagnetism, yet orders antiferromagnetically at a wave vector unrelated to Fermi surface nesting. We show that mirrored vHs provide the long-wavelength, low-frequency fluctuations characteristic of a wFM rather than that of a conventional wAFM, whereby wAFM competes on equal terms with wFM for the broken symmetry ordered state. Peierls-like energy gain from cell doubling can help promote wAFM, which is evident in TiAu.

Background. – Weak itinerant ferromagnets (wFMs), conventionally understood as stoichiometric compounds comprised of elements not displaying local moments themselves, are few, and command attention for that reason as well as for their existence at the extreme. Their sister weak *anti*ferromagnetic systems (wAFM) are practically nonexistent, making the recent identification [1] of the wAFM TiAu a phenomenon in need of understanding. wFM phenomena and materials, reviewed recently [2], provide one of the main platforms to study quantum-critical points, where ordered phases (most often magnetic) appear or vanish at second order, or weakly first-order, phase transitions, accessed by tuning such as by doping or pressure. These long-wavelength (wave vector $\vec{q} \to 0$) processes are displayed in an assortment of materials [2], with some of the prominent examples being understood in terms of the Stoner instability of the nonmagnetic phase [3,4]. In terms of the magnetic exchange coupling I of states at the Fermi surface (FS), and the Fermi level (E_F) density of states $N(E_F)$, if $IN(E_F) > 1$ the itinerant system can sacrifice increased kinetic energy by a gain in exchange (magnetic) energy, and ferromagnetism – possibly weak – becomes the stable phase. The theory of such phases including the quantum-critical and thermal fluctuations attending the small order parameter, is well developed by Moriya and collaborators [5–8], Hertz [9], Millis [10], and several others since [2,11].

We address here not critical phenomena but rather the underlying origin of the electronic instability. Moriya's self-consistent renormalization (SCR) theory of spin fluctuations [7] provides a useful guide for our purposes, as it ties the small ω, small $q \equiv |\vec{q}|$ (for wave vectors $\vec{Q}+\vec{q}$ near the ordering wave vector $\vec{Q}$) behavior to averages of various Fermi surface quantities, thus bringing the focus to the geometry, topology, velocity, and effective mass fields of the FS. wAFMs, and their spin density wave (SDW) cousins, have been discussed theoretically almost exclusively in terms of FS nesting [12,13], and the SDW cases generally support that mechanism. TiAu, however, appears to present its strongest nesting [1] at an incommensurate wave vector that is well separated from what is observed. An added conundrum is that the Fermi energy in TiAu lies almost exactly on a sharp, narrow van Hove singularity (vHs) peak in $N(E)$ that implies a Stoner instability, in which case *ferro*magnetism or possibly superconductivity, rather than wAFM, is expected to emerge. We have found, however, that a re-analysis of the susceptibility accounting for mirrored vHs and techniques based on first density functional theory can resolve these conundrums, revealing an unanticipated mechanism of AFM ordering in itinerant systems.

Properties of TiAu. – TiAu, space group *Pmma* (#51), is orthorhombic with two formula units (f.u.) per

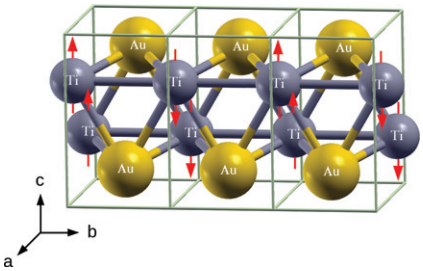

Fig. 1: (Color online) Structure of *Pmma* TiAu with two f.u. per primitive cell (outlined). Antiferromagnet ordering with modulation vector $Q = (0, \frac{\pi}{b}, 0)$ is shown. The positions of Ti and Au are at $2e$ (0.25, 0, 0.3110) and $2f$ (0.25, 0.5, 0.8176) sites, respectively.

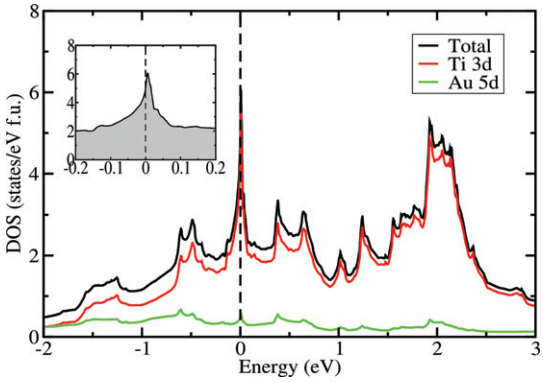

Fig. 2: (Color online) Density of states in the Ti $3d$ band region, displaying the very sharp van Hove singularity peak rising by a factor of three above the background (see inset) and nearly coinciding with the Fermi level. Inset: the narrow and high peak in the DOS, lying 4 meV above the Fermi level.

cell, with lattice constants $a = 4.622\,\text{Å}$, $b = 2.915\,\text{Å}$, $c = 4.897\,\text{Å}$ (see fig. 1). It orders antiferromagnetically at $T_N = 36\,\text{K}$, and neutron diffraction identifies a commensurate wave vector $\vec{Q}^{AFM} = (0, \pi/b, 0)$ and an ordered moment of only $0.15\mu_B$/Ti [1]. The magnetic susceptibility follows a Curie-Weiss (CW) form over a wide temperature range with CW moment of $0.8\mu_B$. This CW moment does not reflect any reasonable local moment (minimal spin-half would give a $1.73\mu_B$ CW moment), but one of the successes of Moriya's SCR theory of itinerant magnetism [6,8] was that the CW temperature dependence should appear, with an apparent moment that is band structure dependent. Another binary Ti compound, $TiBe_2$, was long discussed as either a wFM or a wAFM, but has finally been classified as an incipient weak magnet [14] (these materials can be extremely sensitive to nonstoichiometry). Why TiAu is a wAFM rather than a wFM, and what is the mechanism given that Fermi surface nesting does not provide the correct wave vector, are the primary issues that lead to a new origin of wAFM.

Methods. – Density functional theory (DFT) calculations have been performed using the all-electron, full-potential local-orbital minimum-basis code (FPLO [15]), in several places comparing results obtained using the local density approximation (LDA) of Perdew and Wang (1992) [16] to those obtained from the generalized gradient approximation (GGA) of Perdew, Burke, Ernzerhof (1996) [17], both in the scalar relativistic limit. Ti $3d, 4s, 4p$ states and Au $5d, 6s, 6p$ states were treated as the valence states. The density convergence with an accuracy of 10^{-6} was chosen as the convergence condition. The self-consistency calculations in this work were performed on a $20 \times 20 \times 20$ k-mesh, and larger meshes were used in analysis.

Electronic structure and energetics. – The DFT atom-projected and total DOS $N(E)$ of TiAu are displayed in fig. 2. The DOS was presented earlier by Svanidze *et al.* [1] and is consistent with our result (which we have converged more highly because we are analyzing the extreme fine structure). The Fermi level E_F lies within the 3 eV wide Ti $3d$ bands, the Au $5d$ bands being fully occupied and well below E_F. The single remarkable aspect of this electronic structure is an extremely sharp and narrow DOS peak 4 meV above E_F, reflecting a strong van Hove singularity (vHs). The large value of $N(E_F) = 9.5$/eV-cell and the strong energy variation nearby, suggests electronic (superconductivity, charge order), magnetic, structural (Peierls), and possibly more exotic instabilities as well as temperature-dependent anomalies.

We calculate the observed AFM phase to be energetically favored by 3 meV/Ti over FM alignment, which itself is 8 meV/Ti lower in energy than nonmagnetic, consistent with observation. The FM moment on Ti is calculated to be 0.84 μ_B within the generalized gradient approximation (GGA) to the exchange correlation energy, consistent with previous findings [1]. It is the AFM moment that should be compared with experiment. Within the local density approximation (LDA), it is $0.45\mu_B$; in GGA, $0.64\mu_B$; the difference reflects the delicacy of the moment in TiAu to the exchange correlation functional. Both values are substantially larger than the observed $0.15\mu_B$, reflecting the semi-local functional (LDA, GGA) that does not account for magnetic fluctuations that reduce the ordered moment. The necessary renormalization and also behavior with both hole and electron doping will be treated elsewhere [18].

The DFT fixed spin moment method [19] was applied to demonstrate the Stoner instability and determine the Stoner interaction constant I, which is well defined within density functional theory as derived and calculated for elemental transition metals by Janak [20]. TiAu is found to be strongly unstable toward ferromagnetism, *i.e.*, the interacting susceptibility from χ from the second derivative of the energy *vs.* magnetic moment $E(M)$ curve is negative. The Stoner product $IN(E_F) = 2.5$, reflecting very strong FM instability. In terms of $N(E_F) = 2.5$ states/(eV-spin-f.u.), the Ti atom in TiAu has $I = 1.06\,\text{eV}$.

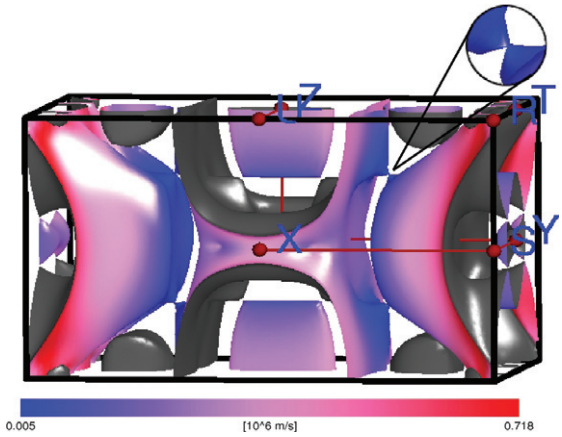

Fig. 3: (Color online) The constant energy surface at $\varepsilon = E_F + 4\,\mathrm{meV}$ reveals the cone-like energy surfaces at the van Hove points. The four vHs in a Brillouin zone are connected by wave vectors $\vec{q} = (0, \pm 0.9\frac{\pi}{b}, \pm 0.98\frac{\pi}{c})$. The velocities range from zero to 7.2×10^7 cm/s.

van Hove singularities. – Probing the vHs reveals an M_1-type singularity (two positive and one negative mass), with energy dispersion relative to the vHs point,

$$\varepsilon_k^{vHs} = \frac{k_x^2}{2m_x} - \frac{k_y^2}{2|m_y|} + \frac{k_z^2}{2m_z}. \qquad (1)$$

Such vHs display a cone-like constant energy surface with a touching point at the vHs energy: $k_y = \pm\sqrt{(m_y/m_x)k_x^2 + (m_y/m_z)k_z^2}$. This cone is visible in the constant energy surface plot at $E_{vHs} = E_F + 4\,\mathrm{meV}$ in fig. 3 (see inset). The positions of the vHs at $(0, \pm 0.45\frac{\pi}{b}, \pm 0.49\frac{\pi}{c}) \equiv (0, \pm K_b, \pm K_c)$ all lie in the $k_x = 0$ plane.

The vHs points are separated by the eight distinct spanning vectors $\{\vec{Q}_{vHs}\} = (0, \pm 2K_b, 0), (0, 0, \pm 2K_c)$, $(0, \pm 2K_b, \pm 2K_c)$, which lie near the zone boundaries. The effective masses at the vHs are surprisingly heavy for an intermetallic Ti-Au compound of this type, $m_x = 21m_e$, $m_y = -4.5m_e$, $m_z = 4.9m_e$, but are consistent with a high DOS peak. The value of $N(E_{vHs})$ and thermodynamic properties are related to the thermal mass $m_{th} \equiv |m_x m_y m_z|^{1/3} = 7.7m_e$, a remarkably large value for an itinerant, presumably weakly correlated, intermetallic compound.

wAFM is addressed in terms of the small ω, small q susceptibility $\chi(Q+q)$ ($\chi = \chi_o + \chi_o I \chi$) relative to the ordering vector Q, as this function describes the low-energy, long-wavelength processes that are the last fluctuations to succumb to order. We focus specifically on the vHs. In the *Pmma* space group the point group consists of all diagonal matrices with ± 1 on the diagonal (half appear with a nonprimitive transition along $\hat{x}$). Since ε_k^{vHs} is even under the mirror operations and rotations are not involved, the vHs energy has the identical form of eq. (1) around each vHs – they all have the same orientation. The spanning vectors Q connect *areas* of Fermi surface rather than simply points.

Fermi surface nesting; vHs mirroring. – The mean-field DFT Kohn-Sham ("Lindhard") susceptibility is

$$\chi_o(\vec{Q} + \vec{q}, \omega) = \sum_{\vec{k},m,n} \frac{f_{\vec{k},n} - f_{\vec{k}+\vec{Q}+\vec{q},m}}{\varepsilon_{\vec{k},n} - \varepsilon_{\vec{k}+\vec{Q}+\vec{q},m} - \omega - i\eta}, \qquad (2)$$

in terms of the Kohn-Sham eigenvalues $\varepsilon_{\vec{k},n}$, and η is a positive infinitesimal. The matrix element factor $|M^{m,n}_{\vec{k},\vec{k}+\vec{Q}+\vec{q}}|^2$ (matrix element of $\exp(i[\vec{Q}+\vec{q}]\cdot\vec{r})$ between Bloch states) has not been displayed as we focus on FS topology, but it is not expected to have any distinctive dependence on q. DFT provides a rigorous formalism [21] for the interacting susceptibility $\chi = \chi_o + \chi_o I \chi$, which is the conventional random phase approximation form, with I defined by Gunnarsson [4] and more generally by Janak [20]. For the case of vHs near or at E_F, the identical vHs dispersions in the $\omega = 0$, $q \to 0$ limit will give a local maximum above the background equal to the density of states from the vHs region (see Supplementary Information `Supplementarymaterial.pdf` (SM)).

Theoretical treatments of wAFM, as well as SDWs, invoke Fermi surface nesting to specify the wave vector of the magnetic order. Svanidze *et al.* observed that the most evident nesting vector (by visual inspection) was not $\vec{Q}^{AFM}$. To address this issue quantitatively, we have evaluated the Fermi surface nesting function $\xi(\vec{q})$ arising for small ω in the imaginary part of dynamic susceptibility $\mathrm{Im}\chi_o(\vec{Q}+\vec{q},\omega) = \pi\omega\xi(\vec{Q}+\vec{q})$ (we set $E_F = 0$) given by

$$\begin{aligned}\xi_{\vec{Q}+\vec{q}} &= \sum_k \delta(\varepsilon_{\vec{k}})\delta(\varepsilon_{\vec{k}+\vec{Q}+\vec{q}}) \\ &= \frac{\Omega}{(2\pi)^3}\int_{\mathcal{L}} \frac{\mathrm{d}\mathcal{L}_{\vec{k}}}{|\vec{v}_{\vec{k}} \times \vec{v}_{\vec{k}+\vec{Q}+\vec{q}}|}. \end{aligned} \qquad (3)$$

The second expression provides the interpretation as the integral over the line of intersection $\mathcal{L}$ of the undisplaced Fermi surface and one displaced by $\vec{Q}+\vec{q}$, weighted by the inverse of the cross-product of the two velocities. Large contributions arise from i) regions of parallel or antiparallel velocities (nesting), or ii) regions where one, or better still both, of the velocities is small (separate from nesting). The former is the classic instance of Fermi surface nesting of parallel pieces of the Fermi surface [13]; recall that $\vec{v}_k$ is perpendicular to the Fermi surface.

The second case is especially pertinent to the vHs in TiAu. Due to mirror symmetries, identical dispersion occurs at each vHs, and the velocities become strictly parallel. In addition, the velocities themselves approach zero, giving a combination of three quantities in the denominator of eq. (3) approaching zero. This confluence represents a strong singularity, modulated only by the finite volume for which the vHs dispersion holds. This volume is larger for heavy effective masses, finally limited by the cubic and higher corrections to the vHs dispersion. The result

(see SM) is that

$$\chi_o(Q+q,\omega \rightarrow \chi_o(Q,0) + \alpha q^2 + i\gamma\frac{\omega}{|q|}, \qquad (4)$$

with band-structure–dependent constants α, γ, and with $\chi_o(Q,0)$ possessing a local maximum proportional to the strength of the vHs. This expression is of the form that Moriya obtained for *ferromagnets*; the $|q|^{-1}$ factor does not appear for conventional antiferromagnets.

Contour plots of the nesting function $\xi(q)$ at the Fermi energy are shown in fig. 4 for each of basal planes $q_z = 0$, $q_x = 0$, $q_y = 0$. The trivial divergence at the zone center as $|\vec{q}| \rightarrow 0$ is not relevant, reflecting as it does the "perfect nesting" when any Fermi surface falls upon itself; physical properties in that limit are regulated by matrix elements and metallic screening. Generically, nesting functions contain ridges of generalized van Hove singularities where parts of the Fermi surface contact or separate as $\vec{q}$ is varied [22]. This delicacy, and the numerical interpolation, account for the wiggly substructure in the contours that have no significance. The peaks in $\xi(\vec{q})$ for TiAu *all occur at vectors that span vHs*, rather than where (visually) Fermi surfaces seem to nest. The latter case ii) above, spanning vHs, causes the peaks in TiAu. Since the spanned vHs have identical dispersions, identically oriented, over a volume of space, when they fall upon one another ($q \rightarrow 0$) there is a $|q|^{-1}$ divergence analogous to that for a generic $\xi(\vec{q})$ in that limit (see SM). However, at nonzero $\vec{Q}$ there are no matrix elements to cancel the divergence – identical (hence degenerate) vHs lead to a physical divergence at the spanning wave vectors. All spanning vectors occur and dominate the structure away from the origin, and they all have similar amplitudes. The divergences are not evident in the figure because that would require a much finer k-mesh to resolve.

Nonlinear aspects of electronic reconstruction. – These results provide a picture of competing magnetic tendencies: the strong FM Stoner instability at $\vec{Q} = 0$, and AFM instabilities at each of the AFM spanning vectors $\{\vec{Q}_{vHs}\}$. The intensities that we calculate lie in the order $\xi(0,0,K_c) > \xi(0,K_b,0) > \xi(0,K_b,K_c)$ but the relative peak heights differ by no more than 5% and matrix elements will differ, so these small differences may not determine the ordering wave vector. The occurrence of a peak at $(0,2K_b,0)$ near $\vec{Q}^{AFM}$ makes the experimental magnetic peak understandable, but does not answer the question why a FM alignment is not more favorable. Our calculations reported above do confirm that the AFM state is lower in energy by a small but significant amount. A more complete evaluation of the susceptibility, with matrix elements and local field factors, could help to understand the relative tendencies but is a formidable task. Also, nonlinear (in magnetic moment beyond the linear response, interacting susceptibility χ) terms in the energy might also be important, as we now address (the paramagnetic susceptibility describes only linear response).

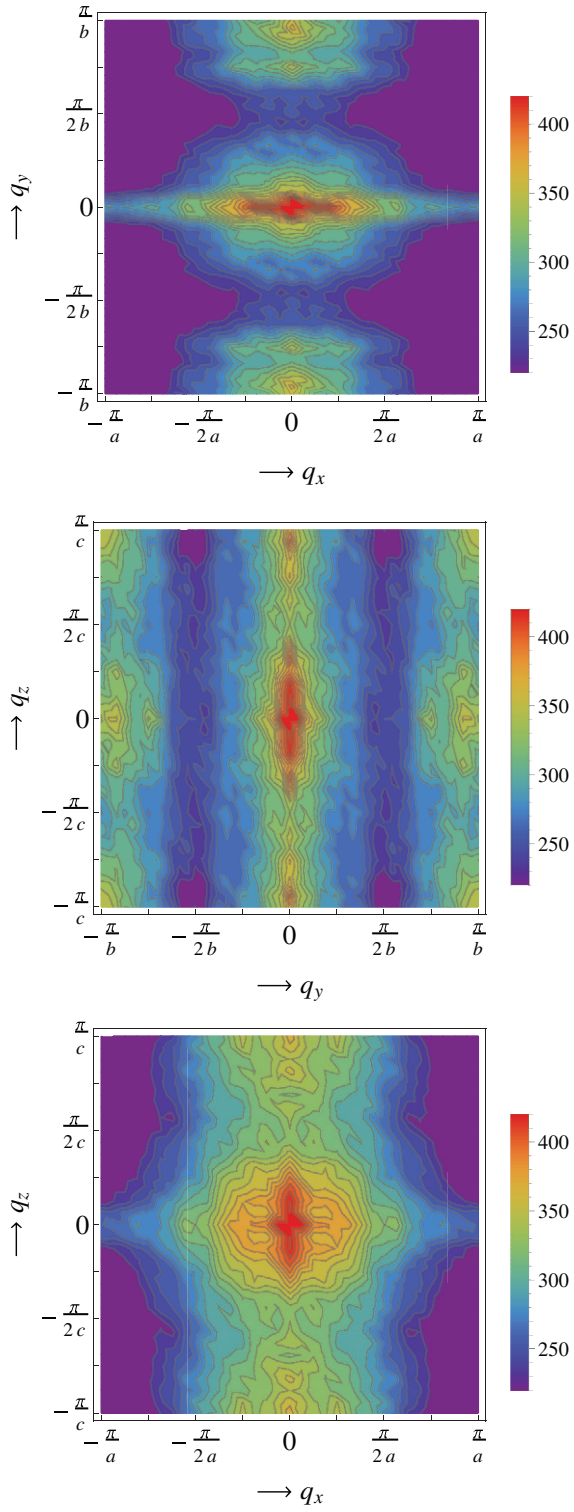

Fig. 4: (Color online) Contour color plot of the Fermi surface nesting function $\xi(\vec{q})$ in the (top to bottom) $q_z = 0$, $q_x = 0, q_y = 0$ planes, respectively. Purple denotes a value less than 220, and the trivial divergence at $\vec{q} \rightarrow 0$ (see text) has been removed by setting the near-divergent values greater than 420 is set equal to 420. The shape of the small $\vec{q}$ contours contains information about the Fermi surface, see the text. The peaks near $(0,\pi/b,0)$ (top), $(0,\pi/b,0),(0,0,\pi/c),(0,\pi/b,0)$ (middle), and $(0,0,\pi/c)$ (bottom) are discussed in the text.

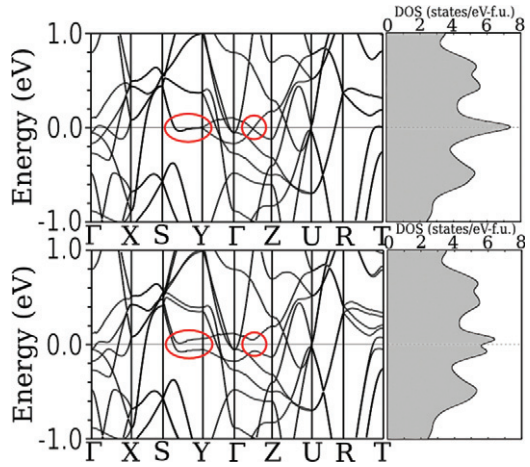

Fig. 5: (Color online) Band structure and DOS of the nonmagnetic (upper panel) and AFM (lower panel) supercell. Symmetry point notations are as in fig. 2, except that now $\vec{b}_{AFM} = 2\vec{b}$. Due to the Ti 3*d* exchange splitting, the doubly degenerate band at the Fermi level along *S*-*Y* is split into majority and minority components above and below E_F, with only the lower one occupied. Bands elsewhere are affected little by the magnetic order.

The wAFM state of TiAu occurs at the commensurate position $\vec{Q}^{AFM}$ rather than at the nearby spanning vectors (of the nonmagnetic bands) $0.90\vec{Q}^{AFM}$ and (by symmetry) $1.10\vec{Q}^{AFM}$, which in the simplest picture would lead to a SDW state with a period of $20b$. A longitudinal SDW loses exchange energy in the regions where magnetization is small, and must make up the energy by gapping the Fermi surface, which is not an uncommon occurrence. However, TiAu does not have nested Fermi surfaces but rather spanned ("nested") identical vHs over a finite but small volume that produce a dynamic instability (divergence of the imaginary part of the magnetic response). Scattering between two such vHs described by a matrix element $\bar{u}_Q$ simply splits the vHs to energies differing by $\pm|\bar{u}_Q|$, reducing the kinetic energy when E_F lies within $\bar{u}_Q$ of the vHs. Since the Ti-Ti separation is shorter in the $\vec{b}$-direction than in the perpendicular directions, the matrix elements, and thus the energy gain, may be larger for $\vec{Q}^{AFM}$ than for the competing spanning vectors.

By slipping to the commensurate wave vector by merging the two incommensurate ones in TiAu, the divergence (at $T \to 0$) of $\chi_o(\vec{Q}, 0)$ is mitigated. Moreover, we find that a flat band at E_F along the zone edge *S*-*Y* line is split by $\vec{Q}^{AFM}$ ordering, providing a Peierls-like band energy gain from unit cell doubling. This band is shown in fig. 5, which also demonstrates how the vHs peak is split leaving E_F in a local minimum. In addition a band crossing along Γ-*Z* at E_F is transformed into an anticrossing, contributing to band energy gain.

Summary. – Effects of scattering between vHs have been discussed in some different contexts. The nearest-neighbor tight-binding model used for high-temperature superconducting cuprates has a vHs at $(\pi/a, 0)$. The sister vHs at $(0, \pi/a)$, is rotated by 90° so the ideal nesting in TiAu does not occur in cuprates. In this regard, the orthorhombic space group of TiAu is important. Also, the vHs in cuprates is two-dimensional, and is discussed as possibly relevant to pairing [23] and to pseudogap behavior [24], *vs.* the AFM ordering in TiAu.

This picture of TiAu provides verifiable predictions. An obvious consequence is Kohn anomalies that should appear in the phonon dispersion at the eight spanning wave vectors above T_N, rather than at $\vec{Q}^{AFM}$. These anomalies should disappear after ordering. Regarding the electronic spectrum, Drozhov has shown that breakdown of the Midgal approximation (electron velocity becoming comparable to, or smaller than, the phonon velocity) leads to vertex corrections that severely alter the electronic spectrum near the vHs position and energy [25]. These effects suggest that investigating properties just above T_N should reveal new behavior related to inter-vHs scattering and the resulting instability.

* * *

We acknowledge helpful conversations with A. S. Botana, S. Gangopadhyay, E. Morosan, Y. Quan, and E. Svanidze. Our research used resources of the National Energy Research Scientific Computing Center (NERSC), a DOE Office of Science User Facility supported by the Office of Science of the U.S. Department of Energy under Contract No. DE-AC02-05CH11231. This work was supported by the National Science Foundation grant DMR-1607139.

REFERENCES

[1] Svanidze E., Wang J. K., Besara T., Liu L., Huang Q., Siegrist T., Frandsen B., Lynn J. W., Nevidomskyy A. H., Gamza M. B., Aronson M. C., Uemura Y. J. and Morosan E., *Nat. Commun.*, **6** (2015) 7701.
[2] Brando M., Belitz D., Grosche F. M. and Kirkpatrick T. R., *Rev. Mod. Phys.*, **88** (2016) 025006.
[3] Stoner E. C., *Proc. R. Soc. London A*, **165** (1938) 372.
[4] Gunnarsson O., *J. Phys. F*, **6** (1976) 587.
[5] Hasegawa H. and Moriya T., *J. Phys. Soc. Jpn.*, **36** (1974) 1542.
[6] Moriya T. and Takahashi Y., *Spin Fluctuations in Itinerant Electron Magnetism* (Springer) 1985.
[7] Moriya T. and Ueda K., *Rep. Prog. Phys.*, **66** (2003) 1299.
[8] Moriya T., *Spin Fluctuations in Itinerant Electron Magnetism* (Springer, Berlin) 1985.
[9] Hertz J., *Phys. Rev. B*, **14** (1976) 1165.
[10] Millis A. J., *Phys. Rev. B*, **48** (1993) 7183.
[11] Löhneysen v. H., Rosch A., Vojta M. and Wölfle P., *Rev. Mod. Phys.*, **79** (2007) 1015.
[12] Enz C. P., *Physica B+C*, **107** (1981) 77.
[13] Fawcett E., *Rev. Mod. Phys.*, **60** (1988) 209.

[14] Jeong T., Kyker A. and Pickett W. E., *Phys. Rev. B*, **73** (2006) 115106.
[15] Koepernik K. and Eschrig H., *Phys. Rev. B*, **59** (1999) 1743.
[16] Perdew J. P. and Wang Y., *Phys. Rev. B*, **45** (1992) 13244.
[17] Perdew J. P., Burke K. and Ernzerhof M., *Phys. Rev. Lett.*, **77** (1996) 3865.
[18] Goh W. F. and Pickett W. E., in preparation.
[19] Schwarz K. and Mohn P., *J. Phys. F*, **14** (1984) L129.
[20] Janak J. K., *Phys. Rev. B*, **16** (1977) 255.
[21] Gross E. K. U. and Kohn W., *Phys. Rev. Lett.*, **55** (1985) 2850.
[22] Kasinathan D., Kunes J., Lazicki A., Rosner H., Yoo C. S., Scalettar R. T. and Pickett W. E., *Phys. Rev. Lett.*, **96** (2006) 047004.
[23] Gofron K., Campuzano J. C., Abrikosov A. A., Lindroos M., Bansil A., Ding H., Koelling D. and Dabrowski B., *Phys. Rev. Lett.*, **73** (1994) 3302.
[24] Markiewitz R. S., Buda I. G., Mistark P. and Bansil A., arXiv:1505.04770.
[25] Drozhov Y. P., *Phys. Status Solidi (b)*, **98** (1980) 781.